Control of triangular formations with a time-varying scale function

Conference Paper *in* Proceedings of the American Control Conference · August 2011

DOI: 10.1109/ACC.2011.5991276 · Source: IEEE Xplore

3 authors, including:

Huang Huang
Beijing Institute Of Control Engineering
11 PUBLICATIONS **63** CITATIONS
SEE PROFILE

Xiangke Wang
National University of Defense Technology
94 PUBLICATIONS **780** CITATIONS
SEE PROFILE

2011 American Control Conference
on O'Farrell Street, San Francisco, CA, USA
June 29 - July 01, 2011

Control of Triangular Formations with a Time-Varying Scale Function

Huang Huang, Changbin Yu, and Xiangke Wang

Abstract— **This paper considers a novel problem of how to choose the scale of the final geometry for three agents in a triangular formation. Instead of assigning a set of desired side lengths, here the only requirement for the desired geometry is a triangle without any location, rotation and, most importantly, scale constraints. We set up a cost function that corresponds to the geometries degree of similarity with respect to the desired shape during convergence, and the cost value is compared between a system with a time varying scale function and the one with a constant scale. A fixed structure nonlinear control law on the positions of agents and the scale function is developed to drive the three agents exponentially converge to a triangle that matches the desired one in a cooperative manner. The control algorithms are validated on three AirRobots. It is shown that system with the proposed time-varying scale function outperforms the one with a constant scale.**

I. Introduction

A group of autonomous agents working together in formation is seen in various field applications including, for example, spacecrafts exploring the deep space, underwater vehicles mapping out oceanbed and unmanned aerial vehicles (UAVs) detecting an unknown territory. A formation system may be characterized by three main design considerations: the geometry of the group of agents, the communication topology [1] and the interaction rules/control algorithms. Most of current research on formation control made the assumption that the desired geometry is specified, fixed, and known a priori, and developed control algorithms including distance-based formation control laws [2], [3], position-based control laws [4]–[6], and very recently, angle-based algorithms [7], [8]. Among those literatures, graph rigidity is crucial to the formation control that is specified by a set of interagent distances, as discussed in [4], [5].

Inspired by the fact that V-shaped formation provides birds with more aerodynamical and visual advantages than other types of flight in flocks [9], it is reasonable to conjecture that the geometry formed by the group of agents is closely related to the behavior of the formation system. One typical example is the angle-based emitter-target localization in sensor networks that emerged in the 1950s. In order to obtain the minimum variance estimation of the target, sensors were expected to be configured under some specific shape constraints [10], say an equilateral triangle. In such a case, the scale of the geometry is flexible. It can be further verified that the geometry with a higher degree of similarity (DOS) (please refer to Section 3 for its definition) to the optimal shape can provide a better target location estimation. Thus *in order to improve the accuracy of measurements on the target before sensors reaching the desired shape so as to allow more time for strategy making, a formation system that maintains a high DOS to the optimal shape during convergence is more preferable than simply focusing on the final shape.*

This problem is closely related to the shape control of formation systems, see [8], [11] and [12]. Also, in [13], the final scale is optimized towards the minimal traveling distance where, however, no cooperation between agents is considered. The design of a specific optimal geometry for a group of wheeled robots is discussed in [14] with the objective of minimizing the overall kinematic energy. What distinguishes our work from the existing ones is that here *we utilize the flexibility on the final scale and design control rules so as to optimize the geometries DOS during convergence*.

Triangular formations with three agents are the most fundamental frameworks in formation systems, and thus are embraced as the starting point in many literatures, see [4], [8], [15], [16].

In order to improve the resemblance of the transient geometry to the desired shape, a metric is expected. The matching of two geometries under rigid transformation has its long history in computer vision. Different metrics of distance between two geometries are proposed from various perspectives where the most famous one is the Hausdorff distance [17]. However, the Hausdorff distance metric is on the basis a minimization function, which is not favorable as an objective function. Meanwhile, at each time step, the time complexity to compute the Hausdorff distance for two points sets of size p and q is $O(pq)$. Thus here we use what we call the DOS determined by the weighted sum of the lengths errors between two geometries to evaluate their resemblance. We exploit the design of a time-varying scale function that provides the optimal rigid transformation (rotation, translation and scaling operations) between two different geometries, and minimize the cost function that is the integration of the transient geometries DOS over the entire convergence process.

An outline of the paper is as follows: Section II contains the notations, definitions and some existing results that are

H. Huang is with the School of Automation, Beijing Institute of Technology, Beijing 100081, China. This work was completed during H. Huang's visit at the Australian National University and was supported in part by the Beijing Education Committee Cooperation Building Foundation Project(XK100070532). huang.huang@anu.edu.au

C. Yu is with the Australian National University and is supported by the Australian Research Council through an Australian Postdoctoral Fellowship under DP-0877562. brad.yu@anu.edu.au

X. Wang is with the College of Mechantronics and Automation, National University of Defense Technology, Changsha, 410073, China. xiangke.wang@anu.edu.au

Correspondence should be addressed to: Changbin Yu, RSISE building 115, The Australian National University, Canberra, ACT, 0200, Australia. Tel.: +61 2 6125 8670; Fax: +61 2 6125 8660

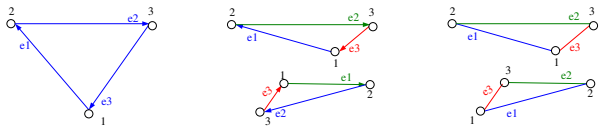

(a) Triangle formation (b) Similar (c) Dissimilar

Fig. 1: Geometries with labeled vertexes

used in the paper. The main results are presented in Section III where we first define the DOS between a geometry and a shape and then setup the problem. Fixed structured nonlinear control law on the scale function is proposed that ensures exponentially convergence to the desired shape. Finally, simulations on three UAVs are demonstrated in Section IV, and conclusions are given in Section V.

II. PRELIMINARIES

A continuous map on space $\mathbb{X}$ is denoted by $C(\mathbb{X})$. $\mathbb{R}^{m\times n}$ is a real matrix of size $m\times n$ where when $n=1$ it is always omitted.

We focus on 2D formations on a plane. Let $\mathbf{z}\in\mathbb{R}^6$ be the coordinates of three labeled points on the plane, as shown in Fig. 1(a), and $\mathbf{e}\in\mathbb{R}^6$ the edge vector with element $e_i\in\mathbb{R}^2$ being the coordinates of the ith edge among the labeled points. When the points are associated with three agents, vector $\mathbf{e}$ is called the *formation* or the *geometry* of the three agents. The set of triangular geometries is denoted by $\mathbb{E}$.

In this paper, two triangles $\mathbf{e}$ and $\mathbf{e}'$ are said to be similar if their labeled edges are in proportion, i.e.,

$$\frac{\|e_i\|}{\|e_1\|}=\frac{\|e_i'\|}{\|e_1'\|}, i=2,3$$

Note that the geometry we considered differs slightly from the general case. Here each vertex in a triangle is labeled from 1 to 3 and two triangles are similar if and only if the corresponding distances between the labeled pairs (viz. labeled edges) are in proportions, as the ones in Fig. 1(b). However the two geometries in Fig. 1(c) are not similar ones due to the swapping of agent 1 and agent 3.

A *shape* consists of geometrical information that remains when location, rotational effects and scale are removed [13]. The shape vector is a three dimensional vector $S=\begin{bmatrix}s_1 & s_2 & s_3\end{bmatrix}^T>0$ with

$$s_i\in\mathbb{R}^+, i\in[1,2,3]$$

All geometries $\mathbf{e}\in\mathbb{E}$ that are similar to the shape S satisfy

$$\|e_i\|=ks_i, k>0, i=1,2,3$$

The set of geometries being similar to the shape S is denoted by $\{\mathbf{e}|S\}$.

In this paper, due to the nature of the algorithm and for simplicity, the scale of a geometry in $\{\mathbf{e}|S\}$ is defined by

$$s=\frac{\|e_i\|^2}{2s_i^2}, i\in[1,2,3]$$

The oriented incidence matrix [18] for the triangular formation system in Fig. 1(a) is

$$H=\begin{bmatrix}-1 & 1 & 0\\ 0 & -1 & 1\\ 1 & 0 & -1\end{bmatrix}$$

By introducing the extended incidence matrix $\hat{H}=H\otimes I_2$, where $\otimes$ denotes the Kronecker product, we have $\mathbf{e}\in\mathrm{Im}\hat{H}$.

The edge lengths are recorded in vector $r(\mathbf{e})$:

$$r(\mathbf{e})=\frac{1}{2}\begin{bmatrix}\|e_1\|^2 & \|e_2\|^2 & \|e_3\|^2\end{bmatrix}^T \tag{1}$$

and its gradient with respect to vector $\mathbf{z}$ is

$$R(\mathbf{e})=\frac{\partial r(\mathbf{e})}{\partial\mathbf{z}}=\Lambda(\mathbf{e})^T\hat{H}$$

with $\Lambda(\mathbf{e})=\begin{bmatrix}e_1 & \mathbf{0} & \mathbf{0}\\ \mathbf{0} & e_2 & \mathbf{0}\\ \mathbf{0} & \mathbf{0} & e_3\end{bmatrix}$.

The following is a result from [5] that concerns the formation control for a fixed final geometry:

Lemma 2.1: For a given distance vector $\mathbf{d}=\begin{bmatrix}d_1 & d_2 & d_3\end{bmatrix}^T$, by choosing the potential function

$$V(\mathbf{e})=\sum_{k=1}^{3}\frac{1}{8}(\|e_k\|^2-2d_k)^2 \tag{2}$$

the control law

$$\dot{\mathbf{z}}=u=-\hat{H}^T[\partial V(\mathbf{e})/\partial\mathbf{e}]^T \tag{3}$$

is an *inverse* optimal solution to the problem

$$\begin{aligned}&\min\bar{J}(\mathbf{e}_0,u)=\frac{1}{2}\int_0^\infty\|R(G)^T[r(\mathbf{e})-d_k]\|^2+\|u\|^2d\tau\\ &\text{s.t. }\dot{\mathbf{e}}=\hat{H}u, \mathbf{e}_0\in\mathbb{E}\end{aligned} \tag{4}$$

where $\mathbf{e}_0$ is the initial geometry of the agents, and the formation system converges to the largest invariant set

$$\mathcal{I}_e=\{\mathbf{e}\in\mathrm{Im}\hat{H}: V(e)\le V(\mathbf{e}_0), \|R(\mathbf{e})^T[r(\mathbf{e})-\mathbf{d}]\|=0\} \tag{5}$$

III. MAIN RESULTS

A. The cost function and the cooperative performance

In this paper, we dive into the convergence process during formation attainment and explore the cooperative performance in terms of the resemblance of a transient geometry $\mathbf{e}(t)$ with respect to the desired shape.

Here are two observations for determining the resemblance of geometries with respect to the reference/desired shape:

i A geometry is less sensitive to perturbations on *longer* edges

ii A geometry is less sensitive to perturbations on edges with larger included angles between $(0,\pi)$

Fig. 2 further explains the above two observations. It is intuitive that under the same perturbation, the longer edge bring smaller deformation to the geometry than that of a short edge, as illustrated in Fig. 2(a). Meanwhile, apart from the lengths of edges, another profile of a triangle is the vertex,

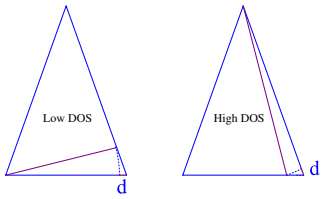

(a) When the short edge (left) suffers a small perturbation, the perturbed geometry various a lot w.r.t. the nominal one; When the same perturbation is added to the long edge (right), the new geometry is quite close to the nominal one

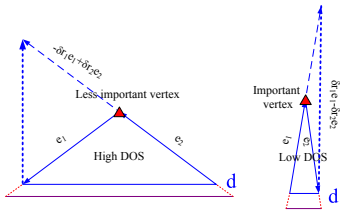

(b) When the inner angle included in the two edges is large (left), perturbations on the two edges will result in small change to the shape; When the inner angle is small (right), the shape is greatly affected by the same perturbation

Fig. 2: The sensitivity of a triangle

especially those sharp vertexes, i.e., the included angle of the two edges adjacent at the vertex is small.

When two geometries are similar to each other, the scale between them is the ratio of two corresponding edges in the geometries and is identical among all the pairs of edges. However, for two dissimilar geometries, there is no common ratio for all pairs of edges, thus choosing an appropriate scale is premise to the analysis of geometries resemblance.

Under observations i and ii, the degree of similarity (DOS) between a geometry $\mathbf{e}$ and a shape S is

$$\begin{aligned} dos_\Theta(\mathbf{e},S) &= \left(\|\hat{H}^T \begin{bmatrix} \delta r_1 e_1 & \cdots & \delta r_n e_n \end{bmatrix}^T \|^2\right)^{-1} \\ &= \left(\| -\delta r_1 e_1 + \delta r_2 e_2\|^2 + \| -\delta r_2 e_2 + \delta r_3 e_3\|^2 \right. \\ &\quad \left. + \|\delta r_1 e_1 - \delta r_3 e_3\|^2\right)^{-1} \end{aligned} \tag{6}$$

where $\delta r_i = r_i - \Theta \bar{s}_i$, $\bar{s}_i = s_i^2$ and Θ is the scaling operation for matching purpose. A geometry's DOS is determined by the weighted vector sum of neighboring edges, which considers both observation i and ii, as illustrated in Fig. 2. A geometry with a higher DOS to S is said to be more resemble to S. When $\mathbf{e}$ is similar to S, $dos_\Theta(\mathbf{e},S) \to \infty$.

Consequently the cooperative performance of the three agents is the integration of geometries DOS over the entire convergence:

$$\begin{aligned} J_v(\mathbf{e}_0,u,\Theta) &= \int_0^\infty dos_\Theta^{-1}(\mathbf{e},S)d\tau \\ &= \int_0^\infty \|R(\mathbf{e})^T[r(\mathbf{e}) - \Theta\bar{S}]\|^2 d\tau \end{aligned} \tag{7}$$

For a special situation when the scaling operation is constant: $\Theta = s_c \in \mathbb{R}^+$, in the authors another paper [19] it is proved that

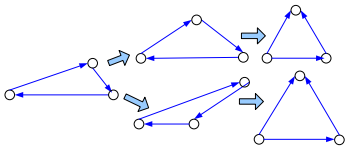

Fig. 3: Cooperative performance

Theorem 3.1: Given a desired shape S, a triangular formation system with control law

$$u(s_c,\mathbf{e}) = -R^T(\mathbf{e})[r(\mathbf{e}) - s_c^*\bar{S}] \tag{8}$$

converges to the invariant set $\{\mathbf{e}|S\}$ exponentially at the minimal cost value $J_v^* = J_v(\mathbf{e}_0,u,s_c^*)$ if and only if

$$s_c^* = \frac{\sum_{i=1}^n \|e_i(0)\|^2 \bar{s}_i}{2\sum_{i=1}^n \bar{s}_i^2} \tag{9}$$

It is intuitive that if we can find an appropriate time-varying scale function that adjusts its value online, the DOS between the current geometry and the desired shape, or the cooperative performance, could be further optimized.

The main concern in this paper is to find an appropriate scale function $\Theta = \tilde{s}(\mathbf{e}), \tilde{s} \in C(\mathbb{E})$ and a control law such that the final geometry of the three agents is similar to S, i.e., $\mathbf{e}_f \in \{\mathbf{e}|S\}$. Thus we formulate the following problem:

Problem 3.1: Consider a formation system with three agents where each agent is modeled by a single integral

$$\dot{\mathbf{z}} = u \tag{10}$$

and the underlying graph G is the one in Fig. 1(a). Consider the following control law on $\tilde{s}(\mathbf{e})$ and $\mathbf{e}$:

$$u(\tilde{s}(\mathbf{e}),\mathbf{e}) = -R(\mathbf{e})^T M(\mathbf{e})^T[r(\mathbf{e}) - \tilde{s}(\mathbf{e})\bar{S}]. \tag{11}$$

Find the control gain $M(\mathbf{e}) \in \mathbb{R}^{3\times 3}$ and the scale function $\tilde{s}(\mathbf{e})$ such that the final geometry $\mathbf{e}_f \in \{\mathbf{e}|S\}$ and

$$J_v^*(\mathbf{e}_0,u(\mathbf{e})) = \min_{\tilde{s}\in C(\mathbb{E})} J_v(\mathbf{e}_0,u(\tilde{s}(\mathbf{e}),\mathbf{e}),\tilde{s}(\mathbf{e})) \tag{12}$$

By minimizing the cost function (7), the two situations as, for example, the ones in Fig. 3, are expected to be distinguished. In sensor networks localization, formation system in the upper case may allow sensors to provide some rough estimate of the target before attaining the desired shape.

Note that J_v is not just quadratic expressions but a function on $\mathbf{e}_0$, u and $\tilde{s}(\mathbf{e})$, thus minimizing the values of J_v is not trivial. Alternatively, we focus on the following suboptimal problem

Problem 3.2: Find a trajectory for $\tilde{s} \in C(\mathbb{E})$ such that $J_v(\mathbf{e}_0,u(\tilde{s}(\mathbf{e}),\mathbf{e}),\tilde{s}(\mathbf{e})) < J_v(\mathbf{e}_0,u(s_c,\mathbf{e}),s_c)$ for all $s_c > 0$.

Consider the equation

$$\frac{\partial J_v(\mathbf{e}_0,u,\tilde{s})}{\partial \tilde{s}} \mid_{\tilde{s}=\tilde{s}^*(\mathbf{e})} = 0 \tag{13}$$

which has the equivalent form of

$$\frac{\partial L}{\partial \tilde{s}} = 2[r(\mathbf{e})^T - \tilde{s}(\mathbf{e})\bar{S}^T]R(\mathbf{e})R(\mathbf{e})^T\bar{S} \tag{14}$$

By using the fact $e_i^T e_j = \|e_i\|\|e_j\| cos\theta_{ij}$ and the cosine law

$$\|e_i\|\|e_j\| cos(\theta_{ij}) = \frac{1}{2}(\|e_i\|^2 + \|e_j\|^2 - \|e_k\|^2)$$

where e_i, e_j and e_k form an triangle, we obtain

$$\frac{\partial L}{\partial \tilde{s}} = 2[r(\mathbf{e}) - \tilde{s}(\mathbf{e})\bar{S}]^T \bar{D} r(\mathbf{e}) \tag{15}$$

where

$$\bar{D} = \begin{bmatrix} \bar{s}_2 + \bar{s}_3 - 4\bar{s}_1 & \bar{s}_2 - \bar{s}_3 & \bar{s}_3 - \bar{s}_2 \\ \bar{s}_1 - \bar{s}_3 & \bar{s}_1 + \bar{s}_3 - 4\bar{s}_2 & \bar{s}_3 - \bar{s}_1 \\ \bar{s}_1 - \bar{s}_2 & \bar{s}_2 - \bar{s}_1 & \bar{s}_1 + \bar{s}_2 - 4\bar{s}_3 \end{bmatrix} \tag{16}$$

If we let $\frac{\partial L}{\partial \tilde{s}} = 0$, a trajectory of $\tilde{s}(\mathbf{e})$ is then

$$\tilde{s}^*(\mathbf{e}) = \frac{r(\mathbf{e})^T \bar{D} r(\mathbf{e})}{\bar{S}^T \bar{D} r(\mathbf{e})} :\triangleq \frac{s_N}{s_D} \tag{17}$$

and we prove that

Theorem 3.2: The inequality

$$J_v(\mathbf{e}_0, u(\tilde{s}(\mathbf{e}), \mathbf{e}), \tilde{s}(\mathbf{e})) < J_v(\mathbf{e}_0, u(s_c, \mathbf{e}), s_c)$$

always holds true for an arbitrary constant value s_c if $\tilde{s} = \tilde{s}^*$ as given by (17).

Proof: Substituting $\tilde{s}^*$ into J_v it yields (for convenience "$(\mathbf{e})$" in $\tilde{s}(\mathbf{e}), R(\mathbf{e}), r(\mathbf{e})$ are omitted)

$$\begin{aligned} & J_v(\mathbf{e}_0, u, \tilde{s}^*) - J_v(\mathbf{e}_0, u, s_c) \\ &= \int_0^\infty (r - \tilde{s}^*\bar{S})^T RR^T (r - \tilde{s}^*\bar{S}) - (r - s_c\bar{S})^T RR^T (r - s_c\bar{S}) \\ &= \int_0^\infty [(\tilde{s}^{*2} - s_c^2)\bar{S}^T + 2(s_c - \tilde{s}^*) r^T] RR^T \bar{S} \\ &= \int_0^\infty (\tilde{s}^* - s_c)(\tilde{s}^*\bar{S}^T - r^T + s_c\bar{S}^T - r^T) RR^T \bar{S} \\ &\triangleq \Delta J_v \end{aligned} \tag{18}$$

Recall the characters of $\tilde{s}^*$ that

$$[r^T - \tilde{s}^*\bar{S}^T] RR^T \bar{S} = 0 \tag{19}$$

and based on the expression of $\tilde{s}^*$ in (17),

$$\tilde{s}^* - s_c = \frac{(r^T - s_c\bar{S}^T)\bar{D} r}{\bar{S}^T \bar{D} r} \tag{20}$$

According to (19) and (20), equation (18) has the simplified form of

$$\Delta J_v = -\int_0^\infty \frac{1}{s_D} \bar{S}^T RR^T (r - s_c\bar{S})(r^T - s_c\bar{S}^T)\bar{D} r$$

The positiveness of s_D is guaranteed according to the equality of

$$\bar{D} r = RR^T \bar{S}$$

which further yields

$$\Delta J_v = -\int_0^\infty \frac{1}{s_D} ((r^T - s_c\bar{S}^T)\bar{D} r)^2 \leq 0, \forall s_c > 0 \tag{21}$$

where equality holds if and only if $s_c \equiv \frac{\|e_i\|^2}{2s_i^2}, \forall i \in [1, 2, 3]$, i.e., $\mathbf{e}_0 \in \{\mathbf{e}|S\}$. ■

Even when $s_c = s_c^*$, the conclusion of $J_v(\mathbf{e}_0, u, \tilde{s}^*)$ having a smaller value still holds true, which indicates that the satisfactory performance is always observed on $J_v(\mathbf{e}_0, u, \tilde{s}^*)$.

Theorem 3.3: The triangular formation system (10) under control law (11) and the scale function (17) is exponentially stable and converges to the largest invariant set $\{\mathbf{e}|S\}$ if

$$M(\mathbf{e}) = s_D^2 I_3 - s_D \bar{S} r(\mathbf{e})^T (\bar{D}^T + \bar{D}) + s_N \bar{S}\bar{S}^T \bar{D} \tag{22}$$

with parameters $\bar{D}$ and s_D, s_N given in (16) and (17) respectively. $\tilde{s}_f^*$ is the stable value of the scale function.

Proof: Consider the positive semidefinite function

$$V(\mathbf{e}) = [r(\mathbf{e}) - \tilde{s}^*(\mathbf{e})\bar{S}]^T [r(\mathbf{e}) - \tilde{s}^*(\mathbf{e})\bar{S}] \tag{23}$$

and its partial differential with respect to $\mathbf{e}$

$$\begin{aligned} \frac{\partial V}{\partial \mathbf{e}} &= 2\frac{\partial [r^T - \tilde{s}^*\bar{S}^T]}{\partial \mathbf{e}} [r - \tilde{s}^*\bar{S}] \\ &= 2[\Lambda(\mathbf{e}) - \frac{\partial \tilde{s}^*}{\partial \mathbf{e}} \bar{S}^T][r(\mathbf{e}) - \tilde{s}^*(\mathbf{e})\bar{S}] \end{aligned} \tag{24}$$

The partial differential $\frac{\partial \tilde{s}^*}{\partial \mathbf{e}}$ is calculated by first solving

$$\frac{\partial s_N}{\partial \mathbf{e}} = \Lambda(\mathbf{e})(\bar{D}^T + \bar{D}) r(\mathbf{e})$$

and

$$\frac{\partial s_D}{\partial \mathbf{e}} = \Lambda(\mathbf{e}) \bar{D}^T \bar{S}$$

which then yield

$$\frac{\partial \tilde{s}^*}{\partial \mathbf{e}} = \frac{s_D \Lambda(\mathbf{e})(\bar{D}^T + \bar{D}) r(\mathbf{e}) - s_N \Lambda(\mathbf{e}) \bar{D}^T \bar{S}}{s_D^2} :\triangleq N(\mathbf{e}) \tag{25}$$

Hence the derivative of $V(\mathbf{e})$ with respect to t is

$$\begin{aligned} \frac{d}{dt} V(\mathbf{e}) &= (\frac{\partial V(\mathbf{e})}{\partial \mathbf{e}})^T \frac{d\mathbf{e}}{dt} \\ &= -2[r(\mathbf{e}) - \tilde{s}^*(\mathbf{e})\bar{S}]^T [\Lambda(\mathbf{e}) - N(\mathbf{e})\bar{S}^T]^T \\ &\quad \hat{H}\hat{H}^T \Lambda(\mathbf{e}) M(\mathbf{e})^T [r(\mathbf{e}) - \tilde{s}^*(\mathbf{e})\bar{S}] \end{aligned} \tag{26}$$

When

$$M(\mathbf{e}) = s_D^2 I_3 - s_D \bar{S} r(\mathbf{e})^T (\bar{D}^T + \bar{D}) + s_N \bar{S}\bar{S}^T \bar{D} \tag{27}$$

the derivative of $V(\mathbf{e})$ in (26) is negatively semi-definite with the expression

$$\begin{aligned} \dot{V}(\mathbf{e}) = & -\frac{2}{s_D^2} [r(\mathbf{e})^T - \tilde{s}^*(\mathbf{e})\bar{S}^T] M(\mathbf{e}) \Lambda(\mathbf{e})^T \hat{H} \\ & \hat{H}^T \Lambda(\mathbf{e}) M(\mathbf{e})^T [r(\mathbf{e}) - \tilde{s}^*(\mathbf{e})\bar{S}] \end{aligned} \tag{28}$$

Indeed, $V(\mathbf{e})$ is a valid Lyapunov function candidate.

For the autonomous system when the derivative of the candidate Lyapunov function is negative semi-definite, the asymptotic stability is concluded based on the powerful invariant set theory.

The set of points in $\mathbb{E}$ when $\dot{V}(\mathbf{e}) = 0$ satisfies both conditions

$$\bar{S}^T \bar{D} r(\mathbf{e}) \neq 0 \tag{29}$$

and

$$\hat{H}^T \Lambda(\mathbf{e}) M(\mathbf{e})^T [r(\mathbf{e}) - \tilde{s}^*(\mathbf{e})\bar{S}] = 0 \tag{30}$$

where condition (29) is always true for a triangle.

When each agents are connected with the other two, matrix $\hat{H}^T\Lambda(\mathbf{e}) \in \mathbb{R}^{6\times 3}$ has rank 3 for all $\mathbf{e} \in \mathbb{E}$.

In order to find the largest invariant set, the singularity of matrix $M(\mathbf{e})$ is crucial to the asymptotic stability. As pointed out in [19], $M(\mathbf{e})$ is a full rank matrix when $r(\mathbf{e}) \neq k\bar{S}$. Thus equation (30) is satisfied if and only if there exist $\mathbf{e}_f$ such that $r(\mathbf{e}_f) = \tilde{s}^*(\mathbf{e}_f)\bar{S}$. Thus $\{\mathbf{e}|S\}$ is the largest invariant set for dynamic system (10) and (11).

If we let ϵ being the smallest eigenvalue of RMM^TR^T during the entire convergence, the derivative of $V(\mathbf{e})$ is bounded by

$$\dot{V}(\mathbf{e}) \leq -\frac{2\epsilon}{\tilde{s}_D^2}\|r(\mathbf{e}) - \tilde{s}(\mathbf{e})\bar{S}\|^2 :\triangleq -\theta$$

which further yields $V(\mathbf{e}) \leq V(\mathbf{e}_0)e^{-\theta}$. According to some trivial calculations, we conclude that $\|r(\mathbf{e}) - \tilde{s}(\mathbf{e})\bar{S}\|$ exponentially converges to zero. ■

Equation (17) is a nonlinear mapping $\tilde{s}^* \in C(\mathbb{E}) : \mathbb{E} \to R$ where the initial edge vector $\mathbf{e}_0$ together with the shape vector S in the nonlinear control law (17) uniquely determine the stable scale $\tilde{s}_f^*$ for the prescribed shape S.

It can be proved that by adding additional control gains at the beginning of the control law (11), the stable scale value $\tilde{s}_f^*$ could be restrained within an interval [19].

The advantages brought by time-varying scale function over constant scale are validated by three UAVs formations demonstrated in the next section.

IV. Quadrotors Formation Flight

We apply the control algorithms on a typical kind of UAV, the AirRobot as shown in Fig. 4. The AirRobot is a quadrotor electrical helicopter with four propellers and a camera. We observe their performance on the Urban Search And Rescue Simulation (USARSim) Platform. Based on the game engine of Unreal Tournament 2004 (UT2004), USARSim is designed as a high fidelity simulation of Urban Search And Rescue (USAR) robots and environments intended as a research tool for the study of Human-Robot Interaction (HRI) and multi-robot coordination. USARSim supports HRI by accurately rendering user interface elements (particularly camera video), accurately representing robot automation and behavior, and accurately representing the remote environment that links the operator's awareness with the robot's behaviors. It has been expanded to support many diverse environments including the DARPA urban challenge, robotic soccer, submarines, humanoids and helicopters.

The workspace of AirRobots is Schönflies space, which is isomorphic to $SO(2) \otimes R^3$. In this paper we validate the algorithms by letting all AirRobots fly at a constant height of $20m$, and thus the problem is reduced to a 2D problem as analyzed in previous sections. We add to each AirRobot a GroundTruth sensor for getting the global coordinates, which can measure position and orientation. The main performances of the AirRobots are listed as follows.

- Dimension(L/W/H): $0.999m/0.999m/0.194m$
- Maximum linear/lateral velocity: 5 m/s

(a) The prototype of the AirRobot

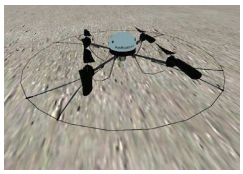

(b) Simulated AirRobot in USARSim

Fig. 4: The AirRobot from AirRobot Co.

(a) $t = 0sec$,$\mathbf{z} = \mathbf{z}_0$
$\{\|e_i\|\} = \{3.04,\ 1.12,\ 4\}$

(b) $t = 4.23sec$
$\{\|e_i\|\} = \{1.03,\ 1.5,\ 0.82\}$

(c) $t = 9.45sec$
$\{\|e_i\|\} = \{1.36,\ 1.23,\ 0.98\}$

(d) $t = 48.2sec$
$\{\|e_i\|\} = \{1.14,\ 1.13,\ 1.15\}$

Fig. 5: Snapshots of AirRobots in formation

The kinematics of a single AirRobot was already implemented in the USARSim platform with flight stabilization control produced by AirRobot Co., thus in the experiments, we focus on their dynamic model, i.e., the velocity of the mass center of each AirRobot. In order to demonstrate the cooperative performance, the convergence process is extended over time by letting each AirRobot move at a constant speed of $0.4m/s$ along x axis and y axis respectively. The position of each AirRobot and the control signals are sampled at a time interval of $0.03s$.

The initial positions of the three AirRobots are $\mathbf{z} = [0; 0; 3; 0.5; 4; 0]$ and the desired shape is an equilateral triangle denoted by $S = [\sqrt{2}; \sqrt{2}; \sqrt{2}]$.

The snapshots of the three AirRobots with the time-varying scale function are demonstrated in Fig. 5. The white dots in the pictures are the three AirRobots. Their trajectories are depicted in Fig. 6(a). The time varying scale function converged to $\tilde{s}_f^* = 0.32$ in less than 9 seconds (1 step=0.03sec).

For system with a time-invariant scale function, the optimal value is calculated at $s_c^* = 2.21$ and the trajectories of the three AirRobots are shown in Fig. 6(b).

In order to show that the time varying scale function results in better cooperative performance than the constant case, we set $s_c \equiv 0.32$, which equals to $\tilde{s}_f^*$ given above, and the trajectories are depicted in Fig. 6(c). The three AirRobots did not converged to a equilateral triangle at $t = 18sec$. Actually it took approximately 30sec for them to get stabilized. The cost values under the three cases are $J_v|_{s_c^*=2.21} = 506.80$, $J_v|_{\tilde{s}^*} = 25.76$ and $J_v|_{s_c=0.32} = 1350$

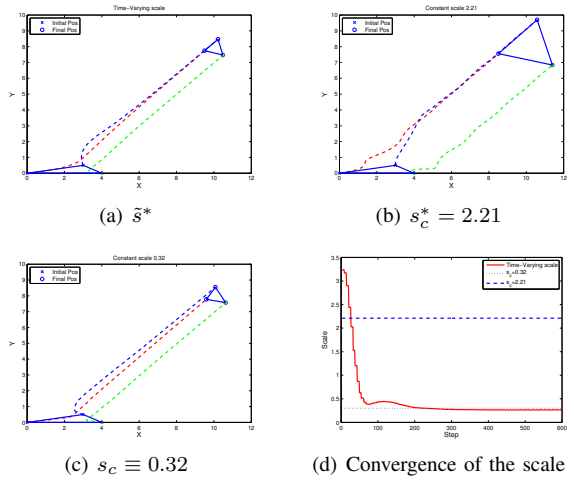

(a) $\tilde{s}^*$ (b) $s_c^* = 2.21$

(c) $s_c \equiv 0.32$ (d) Convergence of the scale

Fig. 6: Three AirRobots formations during $t = [0, 18]sec$ and the curve of the scale function

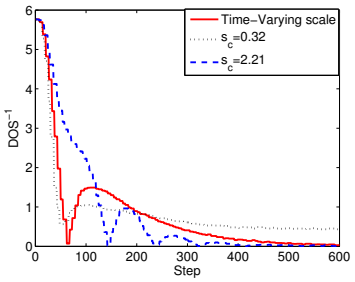

Fig. 7: The inverse of DOS over time

respectively, which validates the conclusion that time varying scale function provides the system with smaller cost value than that of a constant scale. The dynamic of the time-varying scale function is shown in Fig. 6(d).

The inverse of the geometries DOS with respect to the equilateral triangle are shown in Fig. 7. The DOS under time varying scale (red line) converged fast and reached the stable value in a relatively short period of time, which indicates that the geometries during convergence have higher DOS to the equilateral triangle. For the constant scale case, it took either a long time to reach the stable point, as for $s_c \equiv 0.32$, or had a bad formation performance during convergence, as for $s_c^* = 2.21$. Due to the inertness of the AirRobot, there were some slight oscillations during convergence.

V. Conclusions and Future Works

In this paper we discussed how to determine the scale of a triangular geometry of a formation system. A cost function that corresponds to the geometries DOS during the convergence was carefully selected. For a group of agents aiming to attain a formation with only shape constraints, we designed the fixed-structured control law and the scale function that ensure the exponential convergence of the three agents to the desired shape. This is a further optimization of the case with a constant scale. The advantages brought by time-varying scale function were validated on three AirRobots in the UASRSim platform, and the feature of the cost function was observed from the experiments.

The triangle ensures the compact form of the partial differential of the value function L due to the cosine law. However, when the number of UAVs exceeds three, this property may not always hold true. In order to generate a similar formula, we found out defining a *triangular complement* graph is the key to the extension. Interested readers are referred to [19] for details.

References

[1] B. D. O. Anderson, C. Yu, B. Fidan, and J. M. Hendrickx, "Rigid graph control architectures for autonomous formations," *IEEE Control Systems Magazine*, vol. 28, no. 6, pp. 48–63, 2008.

[2] B. D. Anderson, C. Yu, S. Dasgupta, and A. S. Morse, "Control of a three-coleader formation in the plane," *Systems & Control Letters*, vol. 56, no. 9-10, pp. 573 – 578, 2007.

[3] D. V. Dimarogonas and K. H. Johansson, "On the stability of distance-based formation control," in *Proceedings of the 47th IEEE Conference on Decision and Control*, 2008, pp. 1200 –1205.

[4] C. Yu, B. D. O. Anderson, S. Dasgupta, and B. Fidan, "Control of minimally persistent formations in the plane," *SIAM Journal on Control and Optimization*, vol. 48, no. 1, pp. 206–233, 2009.

[5] F. Dörfler and B. Francis, "Formation control of autonomous robots based on cooperative behavior," in *Proceedings of the European Control Conference 2009*, Budapest, Hungary, 2009, pp. 2432–2437.

[6] W. Ren and N. Sorensen, "Distributed coordination architecture for multi-robot formation control," *Robotics and Autonomous Systems*, vol. 56, no. 4, pp. 324–333, 2008.

[7] N. Moshtagh, N. Michael, A. Jadbabaie, and K. Daniilidis, "Vision-based, distributed control laws for motion coordination of nonholonomic robots," *IEEE Transactions on Robotics*, vol. 25, no. 4, pp. 851 –860, 2009.

[8] M. Basiri, A. N. Bishop, and P. Jensfelt, "Distributed control of triangular formations with angle-only constraints," *Systems & Control Letters*, vol. 59, no. 2, pp. 147 – 154, 2010.

[9] H. Weimerskirch, J. Martin, Y. Clerquin, P. Alexandre, and S. Jiraskova, "Energy saving in flight formation," *Nature*, vol. 413, no. 6857, pp. 697– 698, 2001.

[10] A. N. Bishop, B. Fidan, B. D. O. Anderson, K. Doğançay, and P. N. Pathirana, "Optimality analysis of sensor-target localization geometries," *Automatica*, vol. 46, no. 3, pp. 479–492, 2010.

[11] D. Pais, M. Cao, and N. Leonard, "Formation shape and orientation control using projected collinear tensegrity structures," in *Proceedings of the 2009 American Control Conference*, 2009, pp. 610 – 615.

[12] B. Nabet, "Dynamics and control in natural and engineered multi-agent systems," Ph.D. dissertation, Princeton University, 2009.

[13] J. Spletzer and R. Fierro, "Optimal positioning strategies for shape changes in robot teams," in *Proceeding of IEEE International Conference on Robotics and Automation*, 2005, pp. 742–747.

[14] R. M. Bhatt, C. P. Tang, and V. N. Krovi, "Formation optimization for a fleet of wheeled mobile robots – a geometric approach," *Robotics and Autonomous Systems*, vol. 57, no. 1, pp. 102 – 120, 2009.

[15] B. D. O. Anderson, B. Fidan, C. Yu, and D. V. D. Walle, "Autonomous UAV formation: Theory and application," in *Recent Advances in Learning and Control*, ser. Lecture Notes in Control and Information Sciences, V. D. Blondel, S. Boyd, and H. Kimura, Eds., vol. 371. Springer, 2008, pp. 15–33.

[16] M. Cao, A. Morse, C. Yu, B. D. O. Anderson, and S. Dasgupta, "Controlling a triangular formation of mobile autonomous agents," in *Proceedings of the 46th IEEE Conference on Decision and Control*, Dec. 2007, pp. 3603–3608.

[17] D. P. Huttenlocher, G. A. Klanderman, and W. A. Rucklidge, "Comparing Images Using the Hausdorff Distance," *IEEE Transaction on Pattern Analysis and Machine Intellegence*, vol. 15, no. 9, pp. 850–863, 1993.

[18] R. Diestel, *Graph Theory*, 4th ed., ser. Graduate Texts in Mathematics. Springer-Verlag, Heidelberg, 2010, vol. 173.

[19] H. Huang, C. Yu, and Q. Wu, "Control of multi-agent formations with only shape constraints," *Submitted*. [Online]. Available: http://arxiv.org/abs/1102.0033